trends in the $^1K_{SeSe}$ coupling constants as compared to those in the observed $^1J_{SeSe}$ coupling constants (see Table I) can be used to rule out the existence of the discrete isomers D and D′ in the sample solution as follows:

In isomers D and D′ the atomic positions 6 and 7 (see Figure 4) are occupied by sulfur. It is easily seen that in both isomers D and D′ the ratio $^1K_{24}/^1K_{12}$ (or symmetry-related $^1K_{35}/^1K_{13}$) should be significantly smaller than 1.00. In the case of the observed spectrum the corresponding ratio $^1J_{24}/^1J_{12}$ (or $^1J_{35}/^1J_{13}$) is clearly over 1.00. The observed trend is approximated by the reduced coupling constants only when the coexistence of different isomers—and their rapid interconversion—is allowed for.

Figure 4 shows a strong dependence of $^2K_{14}$ (or $^2K_{15}$) on the conformation. In the chair conformation this coupling has a large positive value, while in the boat conformation it is slightly negative. Since the observed coupling over two bonds is smaller in 1,2,3,4,5-Se_5S_2 than in 1,2,3,4,5-Se_5S_3 (see Table I), this seems to indicate that rapid interconversion of isomers with both conformations is taking place in the solution.

Conclusions

The ^{77}Se NMR spectrum of the fluxional 1,2,3,4,5-Se_5S_2 (94% enrichment with ^{77}Se isotope) shows three second-order multiplets, which can be assigned in terms of the five-spin [AMM′XX′] system. The simulation of the spectrum yields all ^{77}Se–^{77}Se coupling constants and enables the complete assignment of all transitions. The number of the NMR signals and their coupling pattern are consistent with the concept of facile pseudorotation in the seven-membered chalcogen-containing ring molecules. The fluxionality is further verified by comparison of the trends in the observed $^1J_{SeSe}$ and $^2J_{SeSe}$ coupling constants to those in reduced coupling constants $^1K_{SeSe}$ and $^2K_{SeSe}$, which indicate that all possible isomers of 1,2,3,4,5-Se_5S_2 in both chair and boat conformations must rapidly interconvert in solution.

Acknowledgment. The financial support from the Academy of Finland is gratefully acknowledged.

Contribution from the Chemistry Department,
University of Virginia, Charlottesville, Virginia 22901

Matrix Infrared Spectra of the Products from Photochemical Reactions of P_4 with O_3 and Decomposition of P_4O_6

Zofia Mielke† and Lester Andrews*

Received November 27, 1989

The P_4/O_3 matrix system has been reinvestigated by using dilute P_4 and a wide range of photolysis wavelengths. With red photolysis the major product is terminal P_4O; with ultraviolet photolysis absorptions for oxo-bridged tetrahedral P_4O and cyclic planar P_4O plus a series of oxo-bridged absorptions leading to P_4O_6 and P_4O_7 dominate. Vacuum ultraviolet photolysis and glow discharge of P_4O_6 produced an absorption for P_4O_7 and three absorptions common to the P_4/O_3 photolysis system, which are assigned to oxo-bridged P_4O_5, P_4O_4, and P_4O_3.

Introduction

Recent infrared studies of matrix reactions of oxygen atoms with P_4 led to identification of two isomers of the lowest phosphorus oxide, P_4O. Red photolysis of the P_4--O_3 complex initiated an oxygen atom transfer reaction, which resulted in terminally bonded P_4O as the major product and oxo-bridged tetrahedral P_4O as a minor product.[1] Since these reactions are highly exothermic, further decomposition or rearrangement reactions, which could lead to smaller molecular fragments or isomerizations, must be considered. Addition of two or more oxygen atoms or ozone molecule(s) to the P_4 cage can lead to other stable oxides of general formula P_4O_x (x = 2–6) where the tetrahedral phosphorus cage is maintained and oxygen atoms form oxo-bridged bonds. In the similar phosphorus–sulfur system, six different tetraphosphorus cage compounds of general formula P_4S_x (x = 3–5) have been characterized.[3-6]

Additional studies of prolonged full-arc photolysis of concentrated Ar/O_3 matrices with dilute P_4 have produced a number of new absorptions in addition to those previously observed.[1] Further ozone photolysis studies were combined with three different discharge experiments where discharged Ar/P_4O_6 mixtures, vacuum UV photolysis of P_4O_6, and reaction between discharged P_4 and ozone have generated novel phosphorus oxides. Comparison of these studies provided identification and structural information on the new phosphorus oxides P_4O_5, P_4O_4, and P_4O_3, which are products of the O_3 photochemical reaction with P_4. The results of these studies are presented here.

Experimental Section

The CTI cryogenics Model 22 refrigerator, Perkin-Elmer 983 spectrometer, high-pressure mercury-arc lamp, and vacuum apparatus and techniques for delivering O_3 and P_4 into matrix samples have been described previously.[1] High-resolution spectra were recorded; wavenumber accuracy is ±0.3 cm^{-1}.

Three different types of discharge experiments were done. In the first studies, an Ar/P_4O_6 mixture was codeposited with argon from a separate 6-mm-o.d. quartz tube, and microwave discharge excitation of the argon provided vacuum UV radiation to the condensing sample. In the second set of experiments, the Ar/P_4O_6 mixture was subjected to low-power discharge. Finally, P_4 from a microwave discharge was codeposited with an Ar/O_3 mixture. A coaxial quartz tube[7] was used in the second and third groups of experiments where a P_4 or concentrated Ar/P_4O_6 mixture was passed through a short (1 cm) argon discharge at the end of an open discharge tube about 5 cm from the matrix window.

The P_4O_6 sample prepared by J. L. Mills was free of impurities on the basis of the matrix infrared spectrum.[2]

Results

Three different types of experiments with two precursor systems produced several common P_xO_y species that will be described below.

$P_4 + O_3$. In the first series of experiments, P_4 was evaporated from white phosphorus at 5–10 °C and codeposited with Ar/O_3 = 200/1, 150/1, 100/1, and 75/1 mixtures onto a 12 K window. Accordingly, the O_3/P_4 ratio was varied over a 3-fold range. Weak product bands, which increased later on photolysis, were observed in the deposited sample, presumably owing to source photolysis. The strong ozone fundamental exhibited a satellite complex band

† On leave from Wroclaw University, Wroclaw, Poland.

(1) Andrews, L.; Withnall, R. *J. Am. Chem. Soc.* **1988**, *110*, 5605.
(2) Mielke, Z.; Andrews, L. *J. Phys. Chem.* **1989**, *93*, 2971 and references therein.
(3) Griffin, A. M.; Minshall, P. C.; Sheldrick, G. M. *J. Chem. Soc., Chem. Commun.* **1976**, 809.
(4) Griffin, A. M.; Sheldrick, G. M. *Acta Crystallogr.* **1975**, *331*, 2738.
(5) Chang, C. C.; Haltiwanger, R. C.; Norman, A. D. *Inorg. Chem.* **1978**, *17*, 2057.
(6) Vos, A.; Olthof, R.; Van Bolhuis, F.; Botterweg, R. *Acta Crystallogr.* **1965**, *19*, 864.
(7) Andrews, L.; Mielke, Z. *J. Phys. Chem.* **1990**, *94*, 2348.

0020-1669/90/1329-2773$02.50/0

Table I. Frequencies of Product Absorptions (cm^{-1}) appearing on Photolysis (220–1000 nm) of $Ar/P_4/O_3$ Matrices and in the Spectra of Discharged Ar/P_4O_6 Mixtures

$P_4 + {}^{16}O_3$		$P_4 + {}^{18}O_3$	$Ar/P_4O_6 + Ar^* h\nu$		$(Ar/P_4O_6)^*$		
ν	A	ν	ν	A	ν	A	identification
					1449.9	0.01	$OPOPO_2$
					1438.2	0.01	$OPOPO_2$
1411.3	0.03	1371.1					$(P_2)(OPOPO_2)$
1378	0.025	1335	1379.5	0.10	1379.9	0.02	P_4O_7
					1325.5	0.04	PO_2
			1319	0.03	1319.0	0.09	PO_2
					1293.0		
					1270.6	0.03	P_2O
1269	0.04	1221					(P_4O_x terminal)
1260.2	0.04	1214.5					$(P_2)(OPOPO_2)$
1240.5	1.20	1201.9					P_4O terminal
1225.8		1188.2					$P_4O\cdots O_2$
1218.8	0.05	1173.6	1218	0.02	1218.4	0.08	PO
1215.7	0.07	1170.6			1215.0	0.04	PO perturbed
1199.6	0.06	1155.6					$(P_3)(PO)$ complex
					1205.1	0.01	PO_2^-
					1198.7	0.01	PO_2^-
					1175.1	0.01	$OPOPO_2$
					1168.0	0.01	$OPOPO_2$
1161.4	0.07	1116.8					$(P_2)(OPOPO_2)$
			1039.7	0.03			O_3
1004.3	0.05				1004.5	0.035	P_4O_8
984.2	0.15	944.0	984.4	0.47	986.3	0.10	P_4O_7
			976.2	0.09			P_4O_7
952.7	0.036	911.7					P_4O_6
941.5	0.07	(905.0)	941.5	0.25	941.6	0.11	P_4O_5
937.6	0.11	900.5	937.7	0.43	937.7	0.11	P_4O_4
			927.4	0.10	926.8	0.03	
915.8	0.14	878.4	915.8	0.31	916.0	0.11	P_4O_3
907.6	0.05	871.1					
897.7	0.10	862.2					(P_4O_2)
891.0	0.10	855.3					(P_4O_2)
			889.5	0.07			
856.0	0.37	821.6					P_4O bridged
			819.7	0.07	840.2	0.02	
830	0.20[a]	795					
802	0.04	769					
770.0	0.05	741.9	770.5	0.17	770.8	0.04	
			706.6	0.05			
			688.6	0.04	688.6	0.01	P_4O_3
668.2		628.8	668.3	0.06	668.7	0.02	P_4O_4
640.6	0.03	611.6					P_4O_6
633.6	0.03	608.0	634.5	0.20	634.8	0.02	P_4O_7
592.2	0.03	570.3					$(P_2)(OPOPO_2)$
553.6	0.04	535.0					P_4O bridged
501.2	0.10	500.7					P_4O terminal
486.8	0.01						$(P_2)(OPOPO_2)$
428.4	0.04	420.3	427.2	0.05			P_4O_7
405.2	0.03	389.7					P_4O_6
350.8	0.01	341.8					$P_2(OPOPO_2)$
329.0		325.6					
244.2	0.10	236.8					P_4O terminal

[a] On full-arc photolysis after deposition, a sharp 827.9-cm^{-1} band appeared here; the ^{18}O counterpart band appeared at 793.4 cm^{-1}.

at 1033.5 cm^{-1}. The samples were photolyzed with a high-pressure mercury arc by using water and glass cutoff filters. Figure 1 presents the spectra from a sample obtained by codeposition of P_4 vapor with a mixture of $Ar/O_3 = 75/1$ followed by photolysis with 630–1000-nm radiation for 10 min, 590–1000-nm radiation for 20 min, 420–1000-nm radiation for 20 min, and 220–1000-nm radiation for 60 min. The frequencies of the bands observed after full-arc photolysis are given in Table I. Absorptions for PO, P_4O, P_4O_6, and P_4O_7 characterized in previous matrix isolation experiments[1,2] are identified in the table and figure; the low concentration of P_4 in the Figure 1 spectra is attested by the weak P_4 absorption at 465 cm^{-1}. Both red photolyses decreased the ozone complex band at 1033.5 cm^{-1}, increased the sharp, strong 1240.5-cm^{-1} P_4O terminal band (labeled 1), the sharp weak absorption at 1203.4 and 1199.6 cm^{-1} (labeled 2), the 952.7-cm^{-1} P_4O_6 band, the 856.0-cm^{-1} P_4O bridged absorption (labeled 3), and sharp weak absorptions at 501.2 and 244.2 cm^{-1} (labeled 1), and produced weak new bands in the 800–1000-cm^{-1} region and at 553.6 cm^{-1} (labeled 3). Photolysis at 420–1000 nm markedly increased the 1 and 3 bands, almost destroyed the 2 band, and produced new bands at 941.5, 937.6, 915.8, 907.6, 897.7 and 891.0 cm^{-1} in the P–O–P stretching region, at 1411.3, 1260.2, and 1161.4 cm^{-1} (labeled Z) in the $-PO_2$ and $-PO$ stretching regions, and at 592.2, 486.8, 428.4, and 350.8 cm^{-1} (labeled Z) in the low-frequency region. All of the above bands increased on full-arc irradiation except the 1 bands, which were unchanged. In some experiments, the $Ar/P_4/O_3$ samples were photolyzed immediately by the full arc; the same products were observed, and a sharp 827.9-cm^{-1} band appeared on top of the broad 830-cm^{-1} absorption.

Concentration and annealing studies showed that the bands in the P–O–P stretching region belong to different species, as their relative intensities changed. Spectra obtained by codeposition of P_4 vapor with $Ar/O_3 = 150/1$ and 100/1 mixtures photolyzed for 60 min with full-arc radiation are compared in Figure 2 for the 1000–800-cm^{-1} region. The relative intensities of these bands

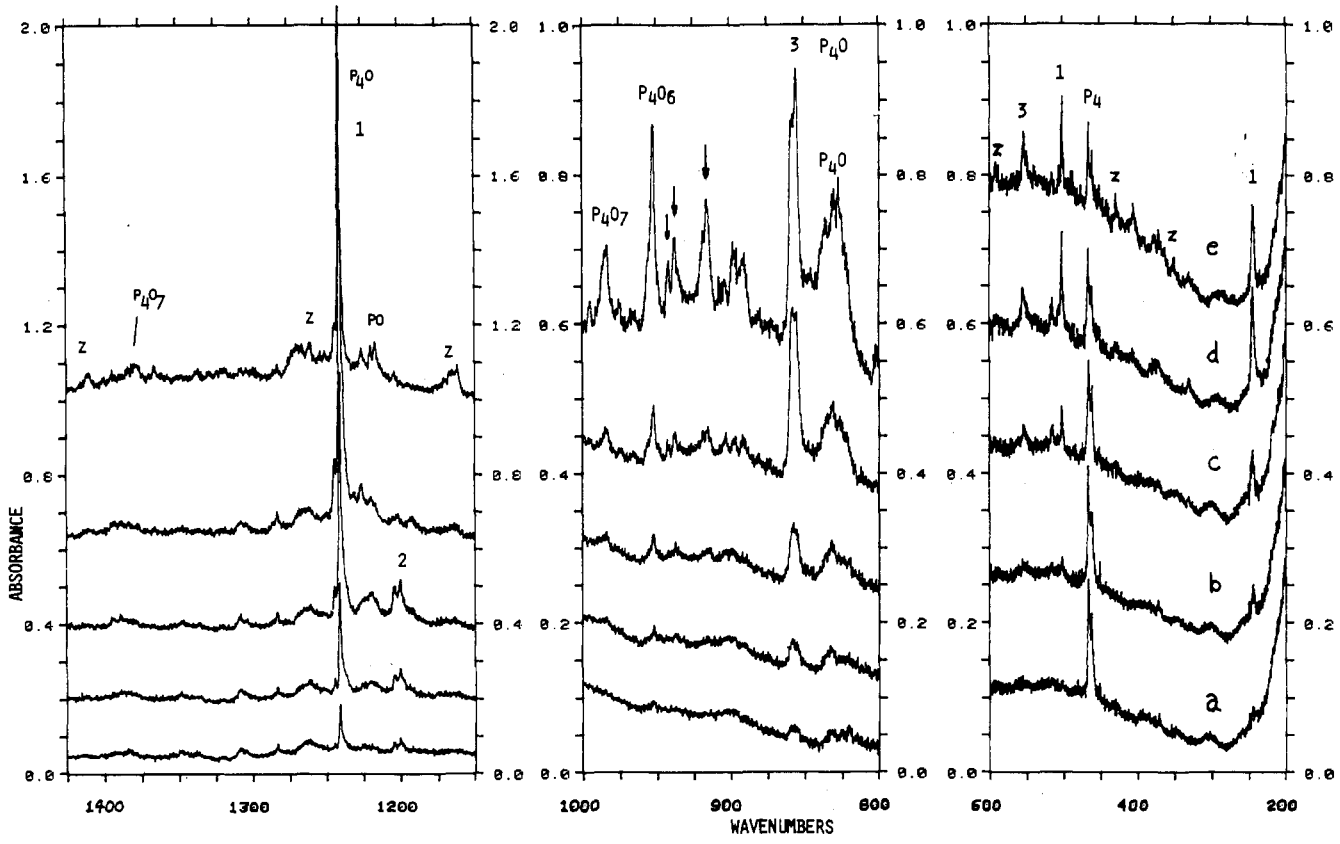

Figure 1. Infrared spectra in three regions for photochemical reaction of O_3 and P_4 in excess argon (a) after codeposition of P_4 vapor from white phosphorus at 6 °C with Ar/O_3 = 75/1 sample for 6 h, (b) after 630–1000-nm photolysis for 10 min, (c) after 590–1000-nm photolysis for 20 min, (d) after 420–1000-nm photolysis for 20 min, and (e) after 220–1000-nm photolysis for 60 min.

depended on O_3 concentration: lower O_3 concentration favored the 856.0-cm^{-1} band, whereas the higher O_3 concentration favored the P_4O_7, P_4O_6, and 915.8-cm^{-1} bands. Figure 2c presents the spectrum of the sample shown in Figure 2b after annealing to 35 ± 2 K for 10 min; the P_4O_7, P_4O_6, and 937.3- and 907.6-cm^{-1} bands and a weak 1004-cm^{-1} band for P_4O_8 (not shown) increased markedly. Figure 3 presents the spectrum in the regions of Z absorptions for a sample of P_4 vapor codeposited with a mixture of Ar/O_3 = 100/1 and photolyzed with 220–1000-nm radiation.

Three experiments were performed with P_4 and $Ar/^{18}O_3$ = 150/1 and 100/1 mixtures. In two experiments, the matrices were photolyzed with 630-, 420-, and 220–1000-nm radiation, and in one experiment the matrix was photolyzed directly with full-arc radiation. After photolysis the matrices were annealed to 30 K for 10 min. The counterpart absorptions were observed for nearly all the bands in $^{16}O_3$ experiments and are listed in Table I. Similar studies were done with P_4 and three $Ar/^{16,18}O_3$ samples; the matrices were photolyzed for 60 min with full-arc radiation. The 1, 3 and 1215.7- and 827.9-cm^{-1} bands appeared as doublets denoting single oxygen atom species. In the P–O–P stretching region, diffuse absorption was observed due to many intermediate mixed-isotope components of vibrational modes involving a large number of oxygen atoms. The 1411.3-cm^{-1} band was split into three components at 1411, 1387, and 1371 cm^{-1}, and the 1161-cm^{-1} band produced a triplet at 1160, 1142, and 1118 cm^{-1}; the 592.2-cm^{-1} band became a broadened doublet at 590 and 571 cm^{-1}.

In a parallel set of experiments, P_4 was passed through the coaxial argon discharge and codeposited with Ar/O_3 samples.[8] The above Z bands appeared on full-arc photolysis, but the 1260.2-cm^{-1} band was not resolved from the strong P_2O band at 1270 cm^{-1}.

Ar/P_4O_6. In the first set of experiments, the Ar/P_4O_6 = 300/1 samples were codeposited with argon passed through the microwave discharge and subjected to argon resonance radiation. The positions of the product absorptions in these experiments are summarized in Table I, and the spectral region of particular interest is shown in Figure 4a. Product absorptions for P_4O_7 and O_3 characterized in previous matrix isolation experiments[2] are identified in Table I. Major new sharp bands were observed at 941.5, 937.7, and 915.8 cm^{-1}, together with weaker bands at 927.4, 889.5, 819.7, 770.5, 706.6, 688.6, 668.3, and 634.5 cm^{-1}. Weak absorptions at 1319 and 1218 due to PO_2 and PO, respectively, were also observed.[1] In a series of experiments with different matrix compositions, Ar/P_4O_6 = 300/1–800/1, which were controlled by argon flow rate with respect to Ar/P_4O_6 flow rate, the 937.7-cm^{-1} band was observed to track together with the 668.7-cm^{-1} band and the 915.8-cm^{-1} band with the 688.6-cm^{-1} band.

In five experiments, the Ar/P_4O_6 = 300/1 mixture was passed through a short argon discharge in a coaxial tube described previously.[7] The positions of the product absorptions in these experiments are also summarized in Table I, and the spectral region of interest is presented in Figure 4b. The product absorptions observed from photolysis of P_4O_6 were also observed here, but the yield of small molecular fragments, PO and PO_2, strongly increased in comparison with larger fragments. In addition, absorptions due to P_4O_8, $OPOPO_2$, P_2O, and PO_2^- were also identified on the basis of their reported spectra.[8] The relative yield of P_4O_6 molecular fragments varied from one experiment to another and was strongly dependent on Ar flow rate with respect to Ar/P_4O_6 flow rate and discharge power, which was varied within the range 30–50%.

Discussion

The lowest oxides of P_4 will be considered, and new absorptions in the oxo-bridged and phosphoryl stretching regions will be identified.

P_4O Isomers. The earlier identification of terminal P_4O was based on the observation of terminal –PO stretching and deformation fundamentals and P_4 cage vibrations.[1] The present studies

(8) Mielke, Z.; McCluskey, M.; Andrews, L. *Chem. Phys. Lett.* **1990**, *165*, 146.

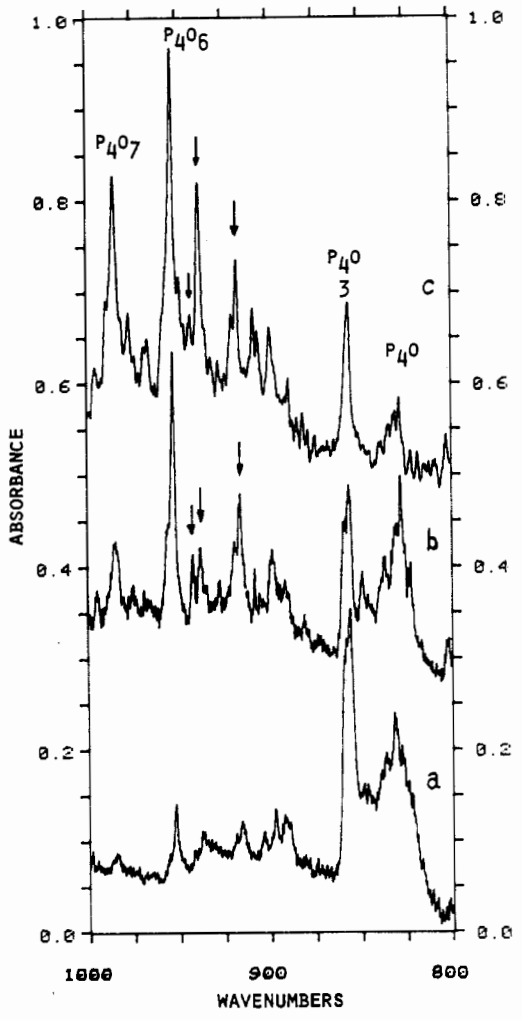

Figure 2. Infrared spectra of matrices obtained by codeposition of P_4 vapor with (a) Ar/O_3 = 150/1 and (b) Ar/O_3 = 100/1 mixtures after 220–1000-nm photolysis for 60 min and (c) mixture b after annealing to 35 ± 2 K for 10 min.

at lower P_4 concentration gave sharper bands and more accurate frequency measurements. Unfortunately, the weaker 603-, 441-, and 393-cm^{-1} bands assigned previously[1] to weaker cage modes of terminal P_4O were not observed in the present experiments and their assignment cannot be confirmed. The strong, sharp, terminal –PO stretching mode (1240.5 cm^{-1}, labeled 1 in Figure 1) shifted to 1201.9 cm^{-1} with ^{18}O (ratio 1.0322) just less than the ratio for a diatomic PO vibration (1.0385). The sharp 501.2-cm^{-1} band above the strongest P_4 band at 465 cm^{-1} is clearly a P_4 skeletal mode perturbed slightly by oxygen as the small 0.5-cm^{-1} ^{18}O shift suggests. The sharp 244.2-cm^{-1} band shifts to 236.8 cm^{-1} with ^{18}O, shows no evidence of splitting, and is assigned to the degenerate –PO deformation mode for the terminal P_4O species of C_{3v} symmetry.

The strongest band at 856.0 cm^{-1} for the oxo-bridged P_4O isomer shifted to 821.6 cm^{-1} with ^{18}O (ratio 1.0419) and the weaker 553.6-cm^{-1} band shifted to 535.0 cm^{-1} (ratio 1.03477). These bands give rise to isotopic doublets in the $^{16,18}O_3$ experiments and are due to antisymmetric and symmetric P–O–P stretching vibrations on the basis of isotopic shift and appearance in the region of P_4O_6 absorptions.[1,2] A strong argument for the formation of bridged P_4O is the progression of bands in the P–O–P stretching region from 891 to 941.5 cm^{-1} leading to oxo-bridged P_4O_6 at 952.7 cm^{-1}.

The sharp product band at 827.9 cm^{-1} in Figure 2b is near a major product absorption at 825.5 cm^{-1} with site splitting at 827.4 cm^{-1} in the $P_2 + O_3$ reactions.[8] These absorptions shifted to 790.2 and 793.0 cm^{-1} with P_2 and $^{18}O_3$ and were assigned to a cyclic planar P_4O isomer in part on the basis of its predicted electronic

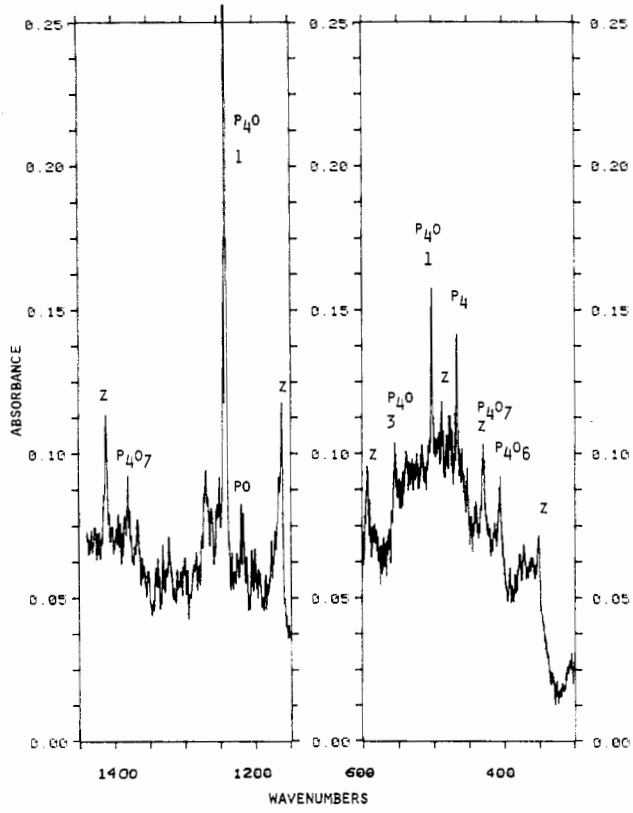

Figure 3. Infrared spectra in the 1450–1150- and 600–300-cm^{-1} regions for a sample of P_4 vapor codeposited with Ar/O_3 = 100/1 and photolyzed with 220–1000-nm radiation for 60 min.

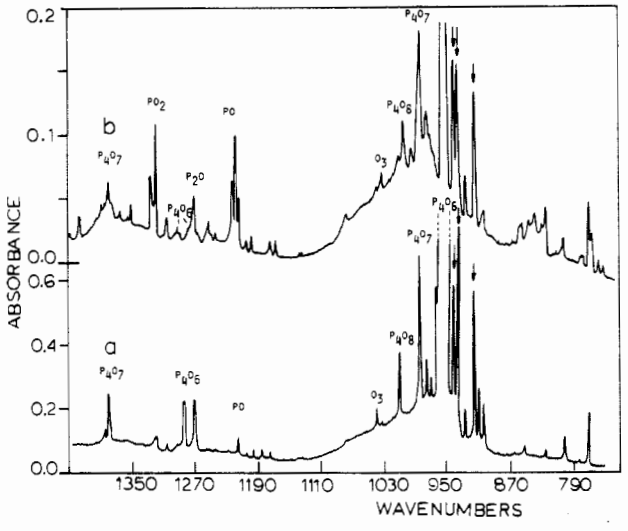

Figure 4. Infrared spectra in the 1450–700-cm^{-1} region of matrix obtained (a) by codeposition of an Ar/P_4O_6 = 300/1 sample with concurrent argon resonance radiation for 6 h and (b) by deposition of an Ar/P_4O_6 = 300/1 sample subjected to low-power discharge.

stability. HONDO 7.0 calculations (DZP basis set) yielded the perhaps surprising result that the cyclic structure is the most stable P_4O isomer yet explored; the cyclic isomer is 7 kcal/mol more stable than the oxo-bridged tetrahedral structure and 30 kcal/mol more stable than the terminal structure.[9] The present 827.9-cm^{-1} band and $^{18}O_3$ counterpart at 793.4 cm^{-1} (ratio 1.0435) are assigned to the antisymmetric P–O–P stretching mode in the cyclic P_4O species as well. The broader band in Figure 1 with an 830-cm^{-1} peak is probably due to the cyclic species as well, where broadening is due to interaction with the O_2 byproduct from ozone photolysis.

(9) McCluskey, M.; Andrews, L. To be published.

P_4/O_3 Photochemistry. The red photochemistry of ozone in complexes has been discussed in detail by Moores and Andrews.[10] Briefly, the red excited state (Chappuis band) for ozone in the complex very efficiently initiates the photochemical reaction. An oxygen atom is transferred from O_2 to Pt either in the red excited electronic state or in high vibrational levels of the ground electronic state of the O_3 submolecule in the complex with P_4. Upon relaxation, the strong new P_4O terminal bond dominates the product distribution in its favor (reaction 1). On the basis of the near

$$P_4\cdots O_3 \xrightarrow[\text{red}]{h\nu} [P_4\cdots O\cdots O_2]^* \xrightarrow{\text{relax}} [P_4O]^* + O_2 \xrightarrow{\text{relax}} \text{terminal } P_4O + O_2 \quad (1)$$

agreement of PO stretching modes for P_4O and diatomic PO (1240 and 1218 cm^{-1}), the PO bond energy (140 kcal/mol)[11] is a good model for the exothermicity of reaction 1. Here the matrix efficiency relaxes the energized species and allows terminal P_4O to be trapped in high yield.

Two P_4 dissociation process are within the energy range, namely $P_4 \rightarrow P_3 + P$, 108 ± 4 kcal/mol, and $P_4 \rightarrow 2P_2$, 55 kcal/mol.[12] Hence, reactions 2 and 3 must be considered. Although it was

$$[P_4O]^* \rightarrow P_2 + P_2O \quad (2)$$

$$[P_4O]^* \rightarrow P_3 + PO \quad (3)$$

first thought that P_2O was a photochemical product of the present reaction,[1] later work with P_2 revealed a different absorption[8,9] for P_2O, and we have no matrix evidence for reaction 2. However, the present 1218.8-, 1215.7-, and 1199.6-cm^{-1} absorptions are due to PO products of reaction 3 on the basis of oxygen isotopic ratios (1.0385, 1.0385, and 1.0381, respectively). The latter band is identified as a $(P_3)(PO)$ complex, which photolyses with 420-nm radiation to give primarily oxo-bridged tetrahedral P_4O. Photoexcitation for reaction 4 occurs through a 427-nm P_3 radical

$$(P_3)(PO) \xrightarrow[\text{blue}]{h\nu} (P_3)^*(PO) \xrightarrow{\text{relax}} \text{bridged } P_4O \quad (4)$$

absorption in solid argon.[7] The former bands are due to isolated and complexed diatomic PO, respectively, and are better resolved after full-arc photolysis.

It is interesting to ponder why reaction 3 contributes a minor decomposition product with red photolysis but reaction 2 does not. Here kinetic factors and activation energy come into play. The average thermochemical bond energy in P_4 (48 kcal/mol)[12] is taken as a means of estimating activation energies for reactions 2 and 3, which require the initial cleavage of four and three P–P single bonds, respectively, in terminal P_4O. Clearly, the former is not possible from the terminal PO bond exothermicity, but the latter is possible when the photon energy (630 nm, 45 kcal/mol) in excess of ozone dissociation (29 kcal/mol)[13] is added.

A small amount of oxo-bridged tetrahedral and planar cyclic P_4O was observed with red photolysis, but the yield increased substantially with ultraviolet irradiation (Hartley band), and little increase in terminal P_4O was observed. Ultraviolet photolysis of ozone gives $O(^1D)$ with high cross section, and $O(^1D)$ apparently prefers the insertion reaction to form a P–O–P bridge bond (reaction 5).

$$P_4\cdots O_3 \xrightarrow[\text{UV}]{h\nu} \text{bridged } [P_4O]^* + O_2 \xrightarrow{\text{relax}} \text{bridged } P_4O + O_2 \quad (5)$$

The rearrangement of excited oxo-bridged tetrahedral P_4O to planar cyclic P_4O before relaxation by the matrix is a straightforward process (reaction 6). The average thermochemical P–O bond energy in P_4O_6 is 86 kcal/mol,[11] which is a useful model for the two single P–O bonds formed in oxo-bridged tetrahedral P_4O from insertion of one O atom. This large exothermicity (172 kcal/mol) can easily provide the activation energy for cleaving the two P–P single bonds in oxo-bridged tetrahedral P_4O required for rearrangement to cyclic planar P_4O, which is the more stable of the two oxo-bridged structures on the basis of ab initio calculations.[9,14] Notice the higher yield of the cyclic planar P_4O rearrangement product as compared to $(P_3)(PO)$ in Figure 1, which is in accord with the substantial exothermicity of reaction 5 over the estimated activation energy for rearrangement (96 kcal/mol) in reaction 6 compared to the small excess exothermicity of reaction 1 over the estimated activation energy for dissociation (144 kcal/mol) in reaction 3.

$$\text{bridged } [P_4O]^* \rightarrow \text{cyclic planar } P_4O \quad (6)$$

P_4O_5, P_4O_4, and P_4O_3 Identification. A set of common, intense bands at 941.5, 937.7, and 915.8 cm^{-1} with accompanying weak bands at 688.6 and 668.7 cm^{-1} observed in P_4/O_3 photolysis and P_4O_6 discharge experiments are assigned to oxo-bridged P_4O_5, P_4O_4, and P_4O_3 species on the basis of the experimental and spectroscopic observations discussed below.

The new 941.5-, 937.7-, and 915.8-cm^{-1} bands were produced in relatively high yield along with P_4O_7, PO_2, and PO in experiments in which the condensing Ar/P_4O_6 mixture was subjected to vacuum UV radiation from discharged argon. In the photofragmentation of P_4O_6, the possible elimination of O atoms, PO, and PO_2 must be considered. The formation of a relatively high yield of P_4O_7 shows that the first step in the P_4O_6 photofragmentation reaction involves elimination of an oxygen atom from P_4O_6 for reaction with another P_4O_6 molecule. The relative yield of PO and P_4O_7 can be estimated from intensities of the bands due to PO stretching modes in the two molecules (assuming similar absorption coefficients for the two bands). The approximate intensity ratio of the two bands $I(1379.6)/I(1218.4)$ is 5/1, which indicates that the P_4O_6 fragmentation channel involving PO elimination contributes less than 20% to the overall fragmentation reaction. The PO_2 concentration (which can be formed by PO oxidation or direct elimination from P_4O_6) was negligible in this experiment. The above data suggest that 941.5-, 937.7-, and 915.8-cm^{-1} absorbing species are formed by elimination of oxygen atoms from P_4O_6. The elimination of one oxygen atom from P_4O_6 leads to P_4O_5, whereas elimination of the second and third oxygen atoms gives P_4O_4 and P_4O_3.

In recent mass spectrometric analysis of vapors over As_4O_6, several thermodynamically stable molecular arsenic oxide species have been identified including As_4O_5, As_4O_4, and As_4O_3.[15] The chemistries of phosphorus and arsenic are similar; in fact, many common oxides of phosphorus and arsenic have been identified (M_4O, M_4O_{6-10}).[1,2,16,17] Like the corresponding arsenic oxides, P_4O_5, P_4O_4, and P_4O_3 are expected to be stable. The same absorptions at 941.5, 937.7, and 915.8 cm^{-1} were observed in P_4/O_3 experiments, which independently confirms their identification as P_4O_n species.

Photochemical changes in the spectra of a $P_4 + Ar/O_3 = 75/1$ sample are shown in Figure 1. Very weak bands in the antisymmetric P–O–P stretching region at 952.7 and 856.0 cm^{-1}, assigned previously to P_4O_6 and oxo-bridged tetrahedral P_4O, were observed after red photolysis. Further blue photolysis revealed an evolution of bands from 856 to 1004 cm^{-1} (see Table I). The product bands include P_4O_8 at 1004 cm^{-1}, P_4O_7 at 984.2 cm^{-1}, the 941.5-, and 937.7-, and 915.8-cm^{-1} bands observed in discharge sampling experiments, and new 897.7- and 891.0-cm^{-1} bands, which grow markedly after full-arc photolysis. The chemical process occurring in the matrix during photolysis involve addition reactions of oxygen atom(s) and/or ozone molecules to the P_4 cage, giving the intermediate oxides, which are expected to occur in the absorption region bracketed by P_4O_6 (952.7 cm^{-1}) and P_4O (856.0 cm^{-1}).

(10) Moores, B. W.; Andrews, L. *J. Phys. Chem.* **1989**, *93*, 1902.
(11) Mellor, J. W. *Inorganic and Theoretical Chemistry*; Wiley-Interscience: New York, 1971; Vol. VIII, Suppl III, Phosphorus.
(12) Bennett, S. L.; Margrave, J. L.; Franklin, J. L. *J. Chem. Phys.* **1974**, *61*, 1647.
(13) Wagman, D. D.; et al. *J. Phys. Chem. Ref. Data* **1982**, *11*, suppl 2.
(14) Lohr, L. L., Jr. *J. Phys. Chem.*, in press.
(15) Brittain, R. D.; Lau, K. H.; Hildebrand, D. L. *J. Phys. Chem.* **1982**, *86*, 5072.
(16) Brisdan, A. K.; Gomme, R. A.; Ogden, J. S. *J. Chem. Soc., Dalton Trans.* **1986**, 2725.
(17) Andrews, L.; Mielke, Z. *Inorg. Chem.* **1989**, *28*, 4001.

Table II. Frequencies of Absorptions Identified for $P_4{}^{16}O_n$ and $P_4{}^{18}O_n$ (n = 3–7) Oxides

P_4O_7			P_4O_6		P_4O_5		P_4O_4		P_4O_3	
^{16}O	$^{18}O_t$	^{18}O	^{16}O	^{18}O	^{16}O	^{18}O	^{16}O	^{18}O	^{16}O	^{18}O
1379	1338	1335								
984.8	*a*	944.9	952.7	913.1	941.5	905.9	937.6	899.8	915.8	878.8
634.6	632.5		640.6	628.8			668.7		688.6	

[a] Obscured by $^{18}O_3$; data from ref 2 for $P_4{}^{16}O_6{}^{18}O$.

Table III. Comparison of the Fundamentals of Species Z and $HOPO_2$, $ClPO_2$, and $OPOPO_2$ Molecules

species Z		$HOPO_2$[a]		$ClPO_2$[b]	$OPOPO_2$[c]		$OPOPO_2$[c]		
$^{16}O_3$	$^{18}O_3$	$^{16}O_3$	$^{18}O_3$	$^{16}O_3$	$^{16}O_3$	$^{18}O_3$	$^{16}O_3$	$^{18}O_3$	identification
1411.3	1371.1	1451.3	1410.8	1448.3	1443.3	1400.9	1450	1408	$\nu_{as}(PO_2)$
1161.4	1116.8	1192.6	1146.7	1145.0	1174.8	1126.2	1033	990	$\nu_s(PO_2)$
		913.4	871.7		955.1	907.6	1008	972	$\nu_{as}(POP)$
1260.2	1214.5								$\nu(PO)$
592.2	570.3								$\nu_s(POP)$
486.8		447.2	426.1	450.0	463.9	442.6	508	493	$\alpha(PO_2)$
428.8	420.3	428.0	419.3		423.8	413.9	428	420	$\omega(OPO_2)$
350.8	341.8	412.0	394.7		371.3	358.0	405	397	$\delta(PO_2)$

[a] Withnall, R.; Andrews, L. *J. Phys. Chem.* **1987**, *91*, 784. [b] Alrichs, R.; Ehrhardt, C.; Lakenbrink, M.; Schunck, S.; Schnockel, H. *J. Am. Chem. Soc.* **1986**, *108*, 3596. [c] Reference 8.

Therefore, the common absorptions occurring in this region at 941.5, 937.7, and 915.8 cm^{-1} both in ozone and discharge sampling experiments, which show appropriate $^{16}O/^{18}O$ ratios (1.042 ± 0.001) for antisymmetric P–O–P vibrations, can be assigned to the intermediate P_4O_{3-5} bridged oxides.

The three absorptions are due to three different species, as can be concluded from their different relative intensities in discharge sampling and ozone experiments and after matrix annealing. On the basis of the O atom and/or O_3 molecule reaction model, the major intermediate species in O_3 photolysis experiments are expected to be P_4O_4 and P_4O_3. The relatively high yield of P_4O_6 in the P_4/O_3 photolysis experiments is most probably due to photochemical reaction of P_4 with two ozone molecules. Similar photochemical reaction between P_4 and one ozone molecule can lead to formation of the P_4O_3 species, and the analogous reaction of P_4O with O_3 can give P_4O_4. The 915.8-cm^{-1} band and accompanying 688.6-cm^{-1} band are assigned to P_4O_3 species. This absorption is more intense after full-arc photolysis than that of other bands in this region. Its growth follows the growth of the 952.7-cm^{-1}, P_4O_6 band suggesting that the corresponding molecule is formed in reaction between P_4 and one O_3 molecule. The 937.6- and 668.7-cm^{-1} bands, which exhibit the most pronounced growth on annealing, are assigned to P_4O_4. The molecule is probably formed in reaction between P_4O and O_3; as can be seen in Figure 2c, the 827.9-cm^{-1} absorption due to cyclic planar P_4O strongly decreases, whereas the 937.6-cm^{-1} absorption strongly increases during matrix annealing. The 941.5-cm^{-1} band, which is less intense than the 937.7- and 915.8-cm^{-1} bands in P_4/O_3 experiments, but of comparable intensity in discharge experiments, is tentatively assigned to P_4O_5. The yield of P_4O_5 species in discharge experiments should be relatively high as its formation requires elimination of one O atom only from P_4O_6 molecule. The 897.7- and 891.4-cm^{-1} bands, not observed in discharge sampling experiments but observed in P_4/O_3 photolysis studies, are tentatively assigned to P_4O_2 species.

P_4O_5, P_4O_4, and P_4O_3 Structure and Comparison. There is only one configuration of the P_4O_5 species if all oxygen atoms are in bridge bonding positions, which is isostructural to the recently isolated β-P_4S_5;[3,4] however, several configurations are possible if one or more oxygen atoms occupy terminal positions. There are two different P_4O_4 configurations with all oxygen atoms in bridging positions, which are isostructural to α-P_4S_4 and β-P_4S_4.[3] The higher stability of the α-P_4S_4 configuration was rationalized on the basis of the rule of topological charge stabilization.[18] Of the three possible P_4S_3 configurations with all S atoms in bridging positions, only one stable P_4S_3 configuration is known, namely that with all three sulfur atoms bonded to one phosphorus atom.[19] The stability of this configuration can also be rationalized on the basis of the rule of topological charge stabilization. According to the same rule, the most stable P_4O_4 and P_4O_3 species should be isostructural with the α-P_4S_4 and P_4S_3 molecules.

The three bands at 941.5, 937.7, and 915.8 cm^{-1} occur clearly in the region of P–O–P antisymmetric stretching vibrations just below the P_4O_6 band at 952.7 cm^{-1}. In a P_4O_{3-5} species with one or more terminal oxygen atoms, a terminal PO stretching vibration would be in the 1280–1380-cm^{-1} region, but no band in this region tracked with the P_4O_{3-5} oxides. Nevertheless, the yield of the P_4O_{3-5} oxides in the matrices studied is large enough for a possible PO stretching mode to be observed. In the spectrum of P_4O_7, the 984.8-cm^{-1} band corresponding to the P_4O_6 cage stretching mode is approximately three times as intense as the 1379.4-cm^{-1} band due to the terminal PO stretching vibration. Accordingly, all oxygen atoms are in bridging positions in the species characterized by the former three bands.

The P_4O_4 molecule with all oxygen atoms in bridging positions is probably isostructural to α-P_4S_4. The two bands assigned to P_4O_4 species at 937.6 and 668.6 cm^{-1} are close to the two most intense P_4O_6 bands at 952.7 and 640.6 cm^{-1}.[2] No other bands were observed for the P_4O_4 molecule, which is probably due to the fact that other absorptions are probably less intense than the two observed bands and to the complexity of the spectra in the region below 1000 cm^{-1}. The 915.8- and 688.6-cm^{-1} bands are tentatively assigned to P_4O_3 species, as discussed earlier. The species is most probably isostructural with the P_4S_3 molecule and has C_{3v} symmetry. The two identified P_4O_3 absorptions are also near the two most intense P_4O_6 bands and correspond to P–O–P antisymmetric and symmetric stretching modes, respectively. The 941.5-cm^{-1} absorption is tentatively assigned to the P_4O_5 molecule, which is isostructural with β-P_4S_5. Table II summarizes the frequencies of the identified modes due to $P_4{}^{16}O_n$ and $P_4{}^{18}O_n$ (n = 3–7) molecules.

Other Secondary Reaction Products. Photolysis of $Ar/P_4/O_3$ matrices with 220–1000-nm radiation produced a new species Z characterized by three bands in the PO stretching region at 1411.3, 1260.2, and 1161.4 cm^{-1} and four weaker bands in the low-frequency region at 592.2, 486.8, 428.8, and 350.8 cm^{-1}. The Z yield was higher in experiments where the matrix was photolyzed first with 220–1000-nm radiation and in experiments with larger O_3/P_4 ratios. It is clear from concentration studies that species Z requires

(18) Gimarc, B. N.; Ott, J. J. *J. Am. Chem. Soc.* **1986**, *108*, 4298.

(19) Hoffman, H.; Becke-Goehring, M. Phosphorus Sulfides. In *Topics in Phosphorus Chemistry*; Griffith, E. J., Grayson, M., Eds.; John Wiley & Sons: New York, 1976; Vol. 8.

P_4 and two O_3 molecules. Unlike the case for oxo-bridged P_4O_x molecules, which increased on sample annealing, the Z absorptions decreased on annealing. A relatively high yield of the Z species was also observed after full-arc photolysis of matrices obtained by codeposition of discharged P_4 and Ar/O_3 mixtures.[8] The frequencies of species Z are presented in Table III and compared with the frequencies of the $ClPO_2$, $HOPO_2$, and $OPOPO_2$ molecules.

The two Z bands observed at 1411.3 and 1161.4 cm^{-1} in the -PO stretching region can be assigned with confidence to antisymmetric and symmetric stretching vibrations of a $-PO_2$ group. Their frequencies and $^{16}O/^{18}O$ isotopic ratios (1.02852 and 1.03975) are close to the frequencies and isotopic ratios of $-PO_2$ groups in the $HOPO_2$, $ClPO_2$, and $OPOPO_2$ molecules (see Table III). The 1411.3-cm^{-1} band was split into a triplet at 1410, 1387, and 1371 cm^{-1}, and the 1161 cm^{-1} band produced a triplet at 1160, 1142, and 1118 cm^{-1}, which show two equivalent oxygen atoms in this $-PO_2$ substituent.

The remaining bands for species Z provide further characterization. The 1260.2-cm^{-1} band (isotopic ratio 1.0376) is appropriate for a terminal -PO fundamental. The 592.2-cm^{-1} band (ratio 1.0384) is in the region of symmetric POP vibrations,[1,2] and although the ratio is a little higher than expected for a pure mode, slight mixing with other vibrations can account for the observed ratio. An associated antisymmetric POP stretching mode could easily be obscured by the strong series of absorptions between 856 and 952 cm^{-1}. As Table III shows, the three lower frequency fundamentals are appropriate for bending, waging, and deformation modes of a $-PO_2$ substituent.

The above information is consistent with a $OPOPO_2$ species. Ab initio calculations by Lohr show that the oxo-bridged structures are more stable than P-P-bonded forms.[20] However, two different configurations of $OPOPO_2$ (noted X and Y) have been characterized in $P_2 + O_3$ and $P_2 + O_2$ studies.[8,9] How does species Z produced from $P_4 + 2O_3$ under full-arc irradiation differ from species X and Y? The obvious difference is the presence of a polarizable P_2 molecule in the adjacent matrix site, which may perturb the structure and/or bonding in the probable $OPOPO_2$ species Z, but formation of another rotational $OPOPO_2$ isomer other than those previously observed cannot be excluded. It should be noted that asymmetrical $OPOPO_2$ species Y bands[8] were observed in experiments with a high yield of species Z.

(20) Lohr, L. L., Jr. *J. Phys. Chem.* **1990**, *94*, 1807.

Conclusions

The products formed by matrix photochemical reaction of P_4 with O_3 and in discharged Ar/P_4O_6 mixtures have been studied in solid argon. The major product of red visible photolysis of the P_4--O_3 complex is terminally bonded P_4O, and minor products are oxo-bridged P_4O and a $(P_3)(PO)$ complex. The major products formed on UV photolysis of $Ar/P_4/O_3$ matrices are the oxo-bridged oxides P_4O_x (x = 1-6) and cyclic planar P_4O.

Full-arc photolysis of concentrated $Ar/P_4/O_3$ matrices and low-power discharge of Ar/P_4O_6 mixtures produced a common set of strong absorptions at 941.5, 937.7, and 915.8 cm^{-1} in the region of P-O-P antisymmetric stretching vibrations. These absorptions are assigned to oxo-bridged P_4O_5, P_4O_4, and P_4O_3 oxides, which are formed by stepwise addition of oxygen atoms and/or O_3 molecule to P_4 in O_3 photolysis experiments and in disproportionation reactions of P_4O_6 and O atom elimination from P_4O_6 in discharge experiments. The relatively high yields of P_4O_4 and P_4O_6 on full-arc photolysis in P_4/O_3 experiments suggest that these molecules are formed by photochemical reaction between P_4 and two ozone molecules trapped in the same matrix site.

Acknowledgment. We gratefully acknowledge financial support from NSF Grant CHE 88-20764, preparation of the P_4O_6 sample by J. L. Mills, and the contribution of preliminary discharge experiments with oxygen and red phosphorus by T. R. Burkholder.

Contribution from the Department of Chemistry, University of Florida, Gainesville, Florida 32611

Free Energies of Electron Attachment to Tris(acetylacetonate) and Tris(hexafluoroacetylacetonate) Transition-Metal Complexes in the Gas Phase: Experimental Results and Ligand Field Analysis

Paul Sharpe, John R. Eyler, and David E. Richardson*,†

Received October 2, 1989

Fourier transform ion cyclotron resonance mass spectrometry was used to investigate gas-phase electron-transfer bracketing reactions and charge-transfer equilibria involving parent negative ions formed from a gas-phase mixture of a metal complex and a reference compound. Estimates of the free energies of adiabatic electron attachment at ~350 K (ΔG_a) for tris(acetylacetonate) complexes ($M(acac)_3$, M = Ti, V, Cr, Mn, Fe, Co, Ru) and tris(hexafluoroacetylacetonate) complexes ($M(hfac)_3$, M = Sc, Ti, V, Cr, Mn, Fe, Co, Ga) are reported. The following values of $-\Delta G_a$ (kcal mol^{-1}) for the process $ML_3(g) + e^- = ML_3^-(g)$ were obtained at ~350 K. $M(acac)_3$ complexes: M = Ti, >0; V, 24.9 ± 0.5; Cr, 20 ± 1; Mn, 59 ± 3; Fe, 43.0 ± 0.5; Co, 47 ± 2; Ru, 38.6 ± 0.5. $M(hfac)_3$ complexes: M = Sc, 64 ± 3; Ti, 69 ± 3; V, 73 ± 2; Cr, 67 ± 3; Ga, 60.4 ± 0.5. From the trends in the experimental data, $-\Delta G_a$ values can be estimated for $Mn(hfac)_3$ (~109 kcal mol^{-1}), $Co(hfac)_3$ (~97 kcal mol^{-1}), and $Fe(hfac)_3$ (~93 kcal mol^{-1}). The trends in energies of electron attachment for the acac complexes are analyzed in terms of ligand field theory. Although the ligand field model provides some insight into the general trends in the thermodynamics of electron capture, the details of the trends in the experimental values of ΔG_a are not modeled effectively.

The thermodynamics of redox processes involving solvated reactants and products are available from electrode potentials, which are related to the free energy change accompanying electron attachment to electroactive species in solution. The trends in electrode potentials for various metal/ligand combinations have typically been treated in a phenomenological manner, since accurate quantum calculations are difficult and solvation energetics are not readily obtained. The value of an electrode potential for a particular metal complex can be considered to be the result of two separate contributions, i.e., the intrinsic gas-phase energy for electron attachment to the complex and the solvation energies for the oxidized and reduced forms.[1] For a particular one-electron redox couple, the thermodynamics of the redox process in the

† A. P. Sloan Research Fellow, 1988-1990.

(1) Buckingham, D. A.; Sargeson, A. M. In *Chelating Agents and Metal Chelates*; Dwyer, F. P., Mellor, P. D., Eds.; Academic Press: New York, 1964; pp 237-282.

0020-1669/90/1329-2779$02.50/0